*Electronic Materials Letters, Vol. 5, No. 1 (2009), pp. 1-6*
DOI: 10.3365/eml.2009.03.001

# Composition and Bonding Structure of Nanostructured Carbon Nitride Films and Their Influences on the Electrical Properties

**Sung Pil Lee***

Department of Electronic Engineering, Kyungnam University,
449, Woryeong-dong, Masan-si, Gyeongnam 631-701, Korea

Carbon nitride films have been deposited by reactive RF sputtering using facing targets. This configuration caused tight confinement of energetic electrons between the targets giving an intense plasma discharge. The surface of carbon nitride films had a good uniformity with a grain size of about 20 to 30 nm. The XPS analysis revealed that the chemical formula of the carbon nitride film could be expressed as $CN_x$ where x is 0.43-0.48. The films had high resistivity and relatively low dielectric constant, the characteristics of which could be expected for use for a new insulating film on the Si fabrication.

**Keywords:** carbon nitride film, sputtering system, facing targets, composition, bonding structure

## 1. INTRODUCTION

In 1985, M. L. Cohen[1] postulated a semi-empirical approach to calculate the bulk modulus of materials. He first applied this approach to group IV, III-V and II-VI tetrahedrally bonded materials. Charge transfer occurs due to repulsive Pauli potential that keeps the valence electrons away from the core region.[2] For example, in $\beta$-$Si_3N_4$ structure, the p electrons in the Si cores repel the valence p electrons, whereas the N cores, which are only s-like, do not contribute strong p repulsion. The result is considerable charge transfer from Si to N and the ionic bonds of the structure become stronger. In the case of $\beta$-$C_3N_4$, charge transfer is not significant, as both C and N have the same core structure. The resulting C-N covalent bond is strong and somewhat similar to the C-C bond in diamond.[2,3] When carbon atoms bond with nitrogen atoms, the structure can have several possible hybridizations: *sp*, $sp^2$, and $sp^3$. Kaufman *et al.*[4] proposed a model for the nitrogen doped carbon solid where nitrogen atoms replace one of the carbon atoms in the carbon-carbon homocyclic ring structure. This proposal allows the $CN_x$ solid to have the C = N $sp^2$ type matrix. A number of models were proposed regarding the bonding nature of this solid.[4-12] The models suggest that a nano-crystalline structure which is predicted as $\beta$-$C_3N_4$ could be formed within the $sp^2$ type C = N matrix. This bonding nature explains the probable mechanical and electrical properties which grade this material in the range of diamond.

Therefore, it is clear that the production of crystalline $\beta$-$C_3N_4$ has been the goal of a lot of research. Although there have been many reports of carbon nitride films of uncertain composition, there have only been a few observations of crystalline $\beta$-$C_3N_4$ produced by reactive sputtering,[7,8] laser ablation[9] and hot filament CVD.[10] Furthermore, the films reported by these reports have been discontinuous with isolated crystals[11] or showing only a few isolated grains in an amorphous matrix.[12] In most cases, high substrate temperatures (600 to 950°C) were required.

In this paper nano-structured carbon nitride films are deposited at relatively low temperature by a reactive magnetron sputtering system using facing targets. We report our investigations on the relationship between the nitrogen content and bonding structure of deposited films as measured by Auger electron spectroscopy (AES), energy dispersive x-ray spectroscopy (EDS), infra-red (IR) absorption and x-ray photoelectron spectroscopy (XPS), and on the effect of these parameters on the electrical properties such as resistivity and dielectric constant.

## 2. EXPERIMENTAL PROCEDURE

Carbon nitride films were deposited on a p-type (100) silicon substrate using the opposed-targets RF reactive sputtering system. This technique differs from the conventional magnetron system in that the two targets are parallel to each other and the magnetic flux lines are oriented along the axis between them as shown schematically in Fig. 1. The use of Nd-Fe-B magnets ensures a very high flux density in the inter-target region. The electrons therefore experience a strong

*Corresponding author: sensors@kyungnam.ac.kr

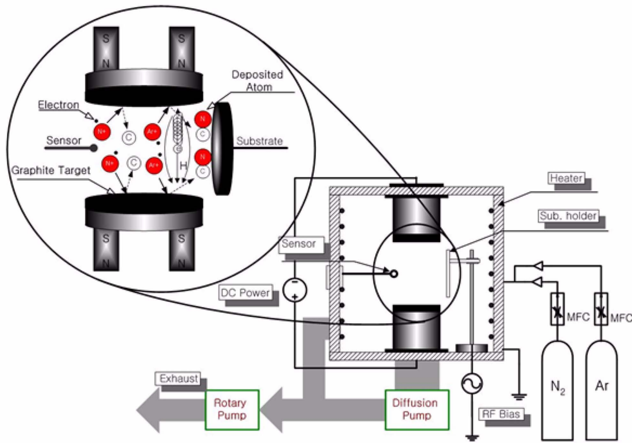


**Fig. 1.** Schematic diagram of a reactive RF magnetron sputtering system with two opposed targets.

magnetic confinement between the two cylindrical targets leading to a very intense ionization in the plasma and a high ion flux at the substrate.

The substrates were ultrasonically cleaned using acetone and methanol before being loaded. Then, they were *in situ* sputter etched in Ar before deposition for 20 min. to remove any surface contamination. The sputtering targets were a graphite of 99.997% purity and the sputter gas was an $Ar/N_2$ mixture of variable composition. The nitrogen (99.999%) gas and the Ar (99.999%) gas were introduced into the sputtering chamber through a mass-flow controller (MFC) until the required pressure was obtained. The nitrogen content of the deposited films was varied by controlling the nitrogen partial pressure in the sputtering gas. The pressure during deposition was $5 \times 10^{-2}$ torr. To avoid any hydrogen contamination from the water molecules on the chamber wall, the chamber was heated to 200 °C with a resistively-heated coil.

To examine the crystal structure of the deposited films, an XRD analysis was performed with an X'pert APD system (Philips, Netherlands) using CuKá radiation ($\lambda = 1.54$) scanning from 10° to 120° of 2 θ. Both the qualitative analysis and the quantitative analysis were carried out using an X-ray Photo Electron Spectroscopy and Auger electron spectroscopy (FISONS MT500, England) with a monochromated MgK (1253.6 eV) x-ray source with an energy resolution of ~0.5 eV. The binding energy values of the photoelectron peaks were measured with an accuracy of ± 0.05 eV. The spectrometer was calibrated to position $4f_{5/2,7/2}$ photoelectron line of clean pure Au foil at a binding energy of 87.74 eV and 84.07 eV. The films were conductive enough to ignore the charging effect. Energy Dispersive X-ray Spectroscopy (EDS, Kevex Sigma MS2, USA) with 138 eV resolution was also used to confirm the quantitative study of the carbon nitride. Heat treatment was carried out at temperatures up to 450°C for 30 min.

## 3. RESULTS AND DISCUSSION

Figure 2 shows the surface and cross-sectional photographs of the deposited carbon nitride film by scanning electron microscopy (SEM). The nano-structured carbon nitride film deposited on Si substrate has a uniform surface morphology. The domain (small grain cluster) size is about 20 to 30 nm and the deposition rate is about 10 nm/min. We can see that SiC and/or SiCN interlayers, as shown in Fig. 2(b), start to form at the interface of Si and carbon nitride film from the reaction of C and N gaseous species with silicon atoms.[13]

Figure 2 Surface (a) and cross sectional (b) SEM photographs of carbon nitride film deposited on the Si substrate (RF power: 300 W, $N_2$/Ar ratio: 70/30, DC bias: -80 V, chamber temperature: 150 °C and deposition time: 20 min.).

Figure 3 shows the XRD spectra of as-deposited carbon nitride films on the Si-wafer with the different RF power. Several experimental data registered in ICDD (International Center for Diffraction Data) were used for references (50-0845, 50-1249, 50-1250, 50-1512).[14-16] All samples show β-$C_3N_4$ (200) and lonsdaleite (102) peaks, i.e. 32.533° (PDF

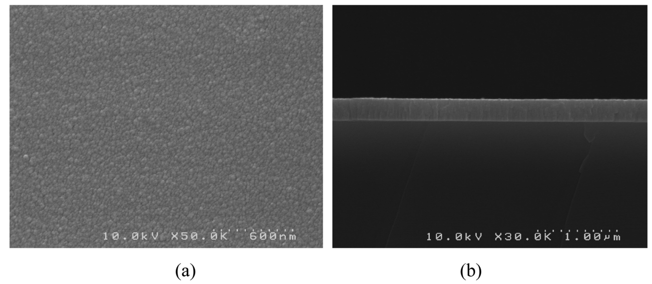


(a) (b)

**Fig. 2.** Surface (a) and cross sectional (b) SEM photographs of carbon nitride film deposited on the Si substrate (RF power: 300 W, $N_2$/Ar ratio: 70/30, DC bias: -80 V, chamber temperature: 150°C and deposition time: 20 min.).

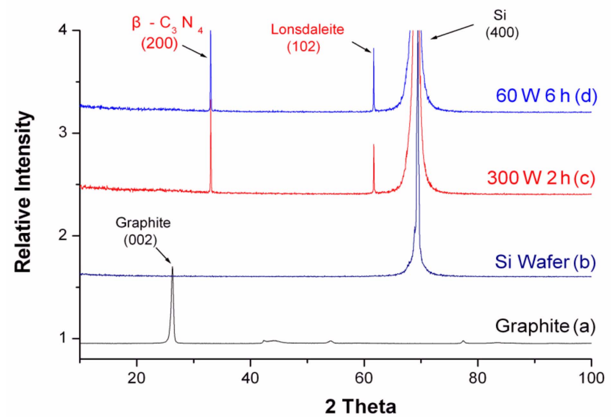


**Fig. 3.** XRD patterns of carbon nitride films with different power; (a) graphite, (b) Si wafer, (c) as deposited carbon nitride film at 300 W for 2 h and (d) as deposited carbon nitride film at 60 W for 6 h.

50-1512) and 61.852° (PDF 19-0268), respectively. The strong peak at 69.19° is the Si (400) peak with d-spacing, 1.3569 Å. There are no graphite peaks in the deposited films. These results reveal that the complete chemical reaction occurred during film formation. As the RF power increases from 60 to 300 W, the lonsdaleite (102) peak decreases slightly. However, we do not observe a considerable change in the β-$C_3N_4$ (200) peak intensity according to RF power.

Figure 3 XRD patterns of carbon nitride films with different power; (a) graphite, (b) Si wafer, (c) as deposited carbon nitride film at 300 W for 2 h and (d) as deposited carbon nitride film at 60 W for 6 h.

To understand the bonding state of the deposited films, we performed the FTIR analysis. Figure 4 shows FTIR spectra of the deposited films as a function the $N_2$/Ar ratio. An absorption peak corresponding to the N-H stretching mode is found in the wave number range of 3000 to 3700 $cm^{-1}$. Seth *et al.*[17] mentioned that the hydrogen incorporation in the CN films resulted in absorption at 3200 and 3365 $cm^{-1}$, owing to the $-NH_2$ symmetric and asymmetric bending modes. They also investigated the hydrogen contamination in CN film by using different chamber pressure. They found that, even though no $H_2$ was introduced into the deposition chamber, absorption bands arising from the CH and NH modes at 2920 and 3365 $cm^{-1}$ appeared in the spectra at nitrogen pressures of 1.5 and 3 mbar. The incorporation of hydrogen in the films is due to (1) the absorbed water on the graphite target, or (2) any contaminations from moderate vacuum (~$10^{-2}$ mbar) conditions in deposition chambers pumped by oil diffusion pump. From Fig. 4, the N-H peak appears strongly as the nitrogen fraction increases. It can be determined that the hydrogen atom reactive with water vapor in the nitrogen gas is more dominant than the out-diffused hydrogen atom from the sputter chamber during deposition; however, the N-H band around 3300 $cm^{-1}$ appears in the spectra for all $N_2$/Ar ratios. This evidence of the presence of N-H bonding suggests that the hydrogen attack occurs not only at the surface but also in the bulk. These spectra show that if hydrogen is present, the nitrile group breaks up and the released nitrogen atom forms N-H bonding. The N-H bonding starts to form in the bulk, due to the sputtering of hydrogen. Hydrogen bonding is commonly seen in porous amorphous materials. As previously reported,[18] when the film is exposed to the air the stress becomes severe. The initial compressive stress becomes more supportive, due to the presence of moisture in the atmosphere.

As the $N_2$/Ar ratio increases, the absorption intensity of the C≡N bond increases at the peak of 2200 $cm^{-1}$. The Si-C peak, which was investigated by the white line between the $CN_x$ film and the substrate in Fig. 2, can be seen at ~816 $cm^{-1}$. The Si (~614 $cm^{-1}$), Si-O (1080~1,100 $cm^{-1}$) and C = N (1500 to 1800 $cm^{-1}$) stretching vibrational modes can also be observed.[19] Rodil *et al.*[20] reported that the amorphous carbon films deposited in pure argon showed broad and weak absorption bands at around 1500 to 1200 $cm^{-1}$ from the Raman spectrum. These were attributed to the Raman-active G (graphite-like $sp^2$ carbon) and D (disordered $sp^2$ carbon) bands, although these should normally be the IR-inactive vibrational modes.[20,21] The absorption bands at around 1200 to 1700 $cm^{-1}$ appear clearly in Fig. 4.

The quantitative analysis of the carbon element and the nitride element was performed by the Gaussian curve fit of XPS binding energy peaks. Figure 5 shows the XPS spectrum of $C_{1s}$ and $N_{1s}$ electrons of carbon nitride films as a function of nitrogen ratio ($N_2/(N_2+Ar)$). The films were deposited with 300 W RF power at 150°C for 1 h. According to the magnified peaks of $C_{1s}$ and $N_{1s}$, the $C_{1s}$ peaks are shifted to the right about 2 eV from β-$C_3N_4$, 286.2 eV[22] and 286.8 eV.[23] However, the $N_{1s}$ peaks are very close to β-$C_3N_4$, 398.6 eV[24] and 398.6 eV.[25] It can be considered that the deposited films are rich in C-C bond. When the $N_2$/Ar are 30/70, 50/50 and 70/30, the nitrogen incorporations are 31.4%, 32.7%, and 34.3%, respectively. The chemical for-

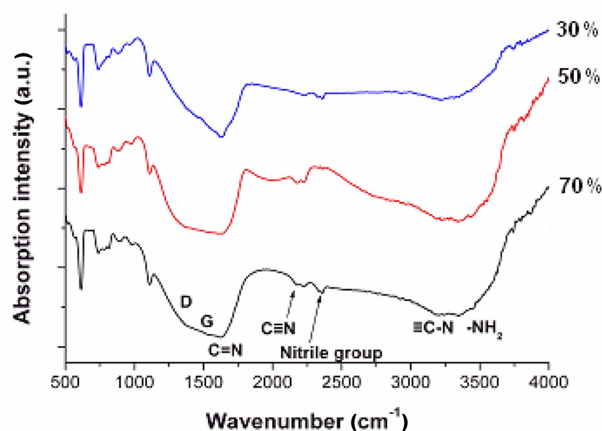


**Fig. 4.** IR absorbance spectrum of the films with different nitrogen fraction; (a) low nitrogen fraction where non hydrogen were traced, (b) high nitrogen fraction deposition where intense N-H stretching band can be observed.

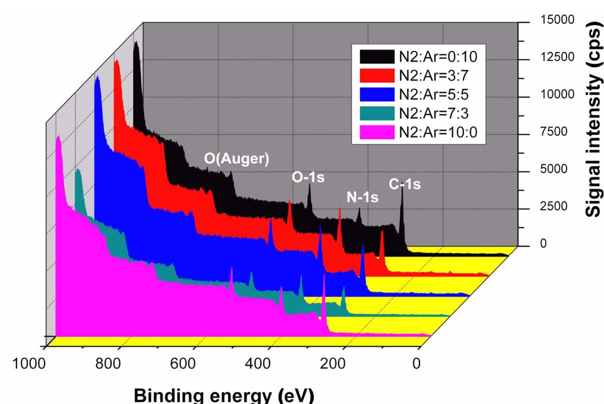


**Fig. 5.** XPS spectra of carbon nitride films as a function of $N_2$/Ar ratio.

mula can be expressed roughly as $CN_x$ where x is 0.43 to 0.48.

The composition ratio of deposited film was also confirmed by EDS which could measure deeper surface than XPS or AES. Figure 6 shows the normalized EDS peaks of the carbon nitride samples. The carbon/nitrogen ratio is 51.97/36.11 at 70% $N_2$ gas. This result is similar to the XPS result. Unwanted nitrogen appears in 0% $N_2$ gas. It shows that carbon nitride around the carbon target is sputtered during the next sputtering process regardless of the pre-sputtering. The detail of the component is shown in Table 1. As the $N_2$ sputtering gas ratio increases, the nitrogen incorporation in the film also increases under the condition that the nitrogen gas ratio is lower than 70%. However, when the $N_2$ ratio is higher than 70%, the nitrogen incorporation is decreased. This is probably due to the increased sputtering rate of C species from the target as the steady state N concentration increases on the target surface. The energetic or neutral Ar species probably enhance the mobility of the nitrogen species and increase the N-sticking at the surface. When the $N_2$/Ar ratio is 30 to 70%, the sticking effect of carbon and nitrogen is maximum at the growth surface. If Ar increases further in the sputtering gas mixture, two things can happen,[9] (1) the sputtering rate of carbon increases with respect to ionized nitrogen species, thus the film contains less nitrogen: (2) chemically enhanced preferential sputtering of nitrogen from the film surface can occur by the energetic Ar species. Increase in Ar gas in the sputter gas mixture may also disrupt the film structure. The momentum of the $Ar^+$ ions is higher than that of either $N_2^+$ or $N^+$ ions, and then the increased momentum transfer into the growing film causes disruption of the bonding structure of the film producing amorphous material. We find that if $N_2$ increases more than 70% in the sputtering gas mixture, the sputtering yield and the N sticking effect are decreased due to deficiency of energetic Ar species.

AES can investigate not only the composition of the film but also the subsurface bonding state with sputtering. Figure 7 shows the atomic composition of carbon, nitrogen and oxygen in the film as a function of deposition time. The films were deposited with 300 W RF and at 150°C. To compare the atomic composition of surface and subsurface, AES was achieved as deposited and after the Ar sputtering for 20 min and/or after the heat treatment at 450°C for 30 min. All films indicate the carbon rich film as well as XPS data. After Ar sputtering, the nitrogen content is reduced but the carbon content is increased as the deposition time is increased. This means that the unstable weak-bonded nitrogen atoms, the dangling bonding for example, exist in the surface of carbon nitride films. However, when the sample is sputtered after the heat treatment at 450°C for 30 min, the atomic contents of carbon and nitrogen are almost the same in the surface and the subsurface because weak-bonded nitrogen atoms in the surface are removed during the heat treatment. The heat treatment leads to a loss of nitrogen from the films at the temperature above approx. 450°C. The loss appears to come preferentially from the less saturated carbon-nitrogen bonds and leads to a softer, weakened film structure. The results indicate that as the heat treatment progresses the C≡N is totally removed at 450°C, the C=N is partially removed and the C-N is not affected.[26] The oxygen content is decreased

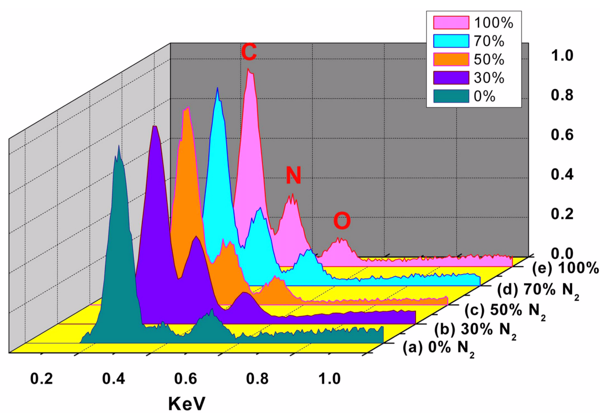


**Fig. 6.** Normalized EDS spectra of carbon nitride films with different $N_2$ ratio.

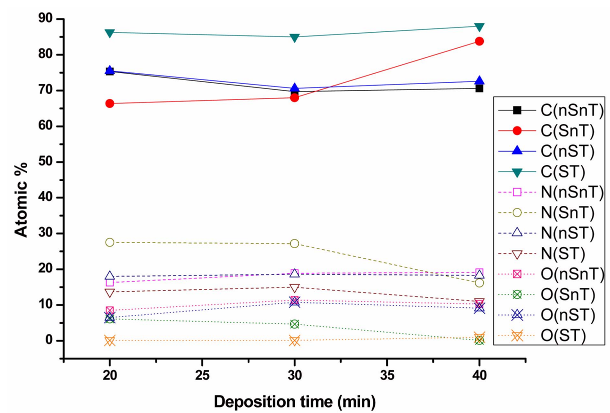


**Fig. 7.** Elemental analysis of carbon nitride films as a function of deposition time; S, T, nS and nT denote sputtering, heat-treated, no sputtering and non heat-treated, respectively.

**Table 1.** Atomic ratio of carbon nitride films by EDS results

| Element \ $N_2$/Arratio | 0/100 | 30/70 | 50/50 | 70/30 | 100/0 |
|---|---|---|---|---|---|
| C | 64.93 at. % | 55.14 at. % | 71.68 at. % | 51.97 at. % | 69.41 at. % |
| N | 4.7 at. % | 31.59 at. % | 32.63 at. % | 36.11 at. % | 24.44 at. % |

slightly after the sputtering because the surface has a lot of carbon and nitrogen bonded with oxygen from water vapor or hydroxyl molecules. In Fig. 7, the heat treatment affects the atomic composition more on the subsurface than on the surface.

Figure 8 shows the resistivity variation of carbon nitride films as a function of nitrogen fraction. As expected in the theoretical prediction, the film has a high resistivity. When the nitrogen fraction is 70%, the resistivity is about $4.5 \times 10^9$ Ω cm. When only Ar is used for the sputtering gas, the semiconducting carbon film that has a relatively low resistivity ($2.4 \times 10^8$ Ω cm) can be formed. It is caused by the decreased sputtering yield due to the deficiency of energetic Ar as mentioned. Then carbon and/or nitrogen vacancies exist in the film.[9] The carriers can be hopped into vacancies easily and the film conductivity should be increased. Under the condition exposed to the humid atmosphere, it is hard to make high resistive film for the insulating layer because of the hydrophilic properties of carbon nitride. If the carbon nitride can be used for an under layer or a buried layer, it could have much higher resistivity.

The presence of the fixed positive charge density located at the insulator-silicon interface and the work function difference between the gate electrode and the silicon substrate will have an effect on the surface space charge region of an MIS capacitor. The amount of gate voltage required compensating for the work function difference between Al and Si substrate in the absence of any interface charge density brings the silicon surface to a flat-band. The barrier height of aluminum on the silicon surfaces is 0.5 to 0.75 eV according to nitrogen fraction. Figure 9 shows the flat-band voltage shift of $Al/C_3N_4/Si$ MIS capacitors at 1 MHz with different nitrogen fractions.

The flat-band condition occurs between the accumulation and depletion conditions. The capacitance at flat-band is given by

$$C_{FB} = \frac{\varepsilon_{CN}}{t_{CN} + \left(\frac{\varepsilon_{CN}}{\varepsilon_{Si}}\right)\sqrt{\left(\frac{kT}{e}\right)\left(\frac{\varepsilon_{Si}}{eN_a}\right)}} \quad (1)$$

where $\varepsilon_{CN}$ and $t_{CN}$ is the dielectric constant and the thickness of carbon nitride, respectively. The voltage shift of the C-V curve is caused by $Q_{CN}$. For a given gate bias and $Q_{CN} = 0$, the depletion layer width is such that the negative charge on the gate is balanced by positive dopant ion charge in the depletion layer. If positive $Q_{CN}$ is introduced into the $Si\text{-}CN_x$ interface, this charge balance is upset. Image charge is introduced in the gate and in the silicon. For the gate, this image charge increases the negative gate charge. For the silicon additional electrons are added at the depletion layer edge, and the depletion layer width is increased. Thus, the capacitance for p-type is smaller than for the ideal capacitor. The result is a shift of the C-V curve to more negative gate bias as seen in Fig. 9. As the nitrogen fraction increases, the flat-band voltage shifts about 1.1 V toward the left. This means that the insulator fixed charge is located more at or very near the $Si\text{-}CN_x$ interface due to the lattice mismatch, as the nitrogen fraction increases. Table 2 shows the dielectric constant of the carbon nitride films with different $N_2/Ar$. The films have a relatively low dielectric constant from 2.97 to 3.14 in the $N_2/Ar$ range of 30/70 to 70/30. These values are lower than that of the dielectric constant of $SiO_2$ (3.9 to 4.2),

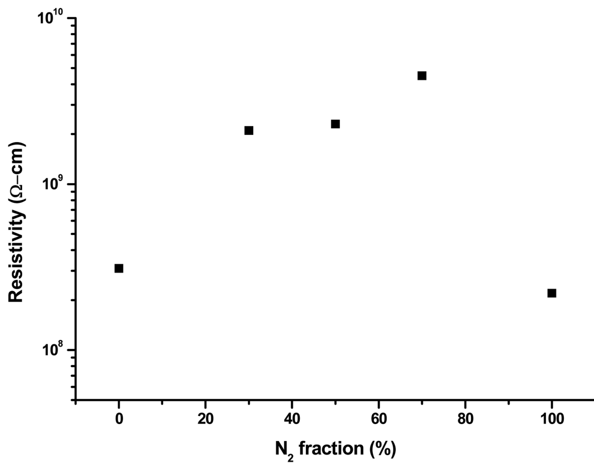


**Fig. 8.** Resistivity changes as a function of the nitrogen fraction at room temperature and 40%RH.

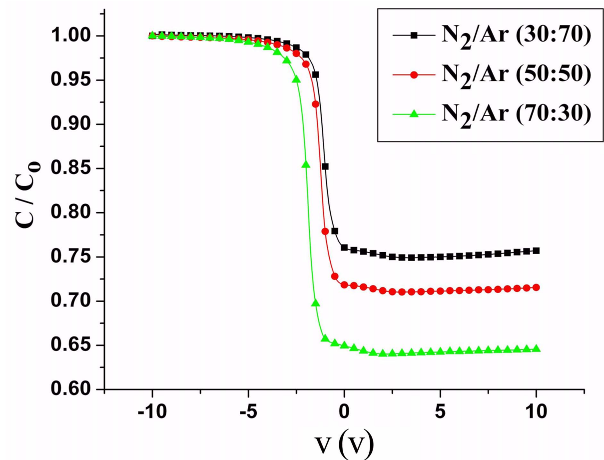


**Fig. 9.** Normalized capacitance-voltage plot of $Al/C_3N_4/Si$ MIS capacitors with different nitrogen fractions.

**Table 2.** Dielectric constant of carbon nitride with different $N_2/Ar$

| $N_2/Ar$ ratio | 0/100 | 30/70 | 50/50 | 70/30 | 100/0 |
|---|---|---|---|---|---|
| Dielectric Constant | 1.15 | 2.97 | 3.03 | 3.14 | 4.33 |

and it is expected that the carbon nitride film can be applied to interlayer insulators for VLSI and ULSI.

## 4. CONCLUSIONS

The nano-structured carbon nitride films were synthesized with a reactive RF magnetron sputtering system with facing targets at different $N_2$/Ar ratios and their electrical properties were investigated. The deposited films showed crystalline β-$C_3N_4$ (200) and lonsdaleite (102) structure and there were no graphite peaks in XRD patterns. The measurements of film composition and IR absorbance showed that for films with less than 30% nitrogen content the nitrogen was mostly bonded to carbon. With increasing nitrogen content above 30%, excess nitrogen was not bonded to carbon but probably exists as N-H bonds. The chemical formula from XPS data of $CN_x$ films that were deposited with 300 W RF power at 150 was expressed as $CN_x$ where x is 0.43 to 0.48, which agreed roughly with EDS. The carbon nitride film had a high resistivity as much as insulators used in semiconductor devices and lower dielectric constant than silicon dioxide. It is expected that the carbon nitride film could be applied to interlayer insulators for VLSI and ULSI.

## ACKNOWLEDGMENT

This research was financially supported by the Ministry of Education, Science Technology (MEST) and Korea Industrial Technology Foundation (KOTEF) through the Human Resource Training Project for Regional Innovation.

## REFERENCES

1. M. L. Cohen, *Phys. Rev. B* **32**, 7988 (1985).
2. M. L. Cohen, *Science* **261**, 307 (1993).
3. Z. Zhong and J. K. Kang, *Electron. Mater. Lett.* **3**, 7 (2007).
4. J. H. Kaufman, S. Metin, and D. D. Saperstein, *Phys. Rev. B* **39**, 13053 (1989).
5. D. Marton, K. J. Boyd, and J. W. Rabalais, *Int. J. Mod. Phys. B* **9**, 3527 (1995).
6. B. C. Holloway, D. K. Shuh, M. A. Kelly, W. Tong, J. A. Carlisle, I. Jimenez, D. G. J. Sutherl, and, L. J. Terminello, P. Pianetta, and S. Hangstrom, *Thin Solid Films* **94-98**, 290 (1996).
7. P. V. Kola, D. C. Cameron, B. J. Meenan, K. A. Pischow, C. A. Anderson, N. M. D. Brown, and M. S. J. Hashmi, *Surf. Coat. Tech.* **74-75**, 696 (1995).
8. N. Nakayama, Y. Tsuchiya, S. Tamada, K. Kosuge, S. Nagata, K. Takahiro, and S. Yamaguchi, *Jpn. J. Appl. Phys.* **32**, L1465 (1993).
9. Z. J. Zhang, S. Fan, J. Huang, and C. M. Lieber, *J. Electron. Mats.* **25**, 57 (1996).
10. D. R. Cole and E. W. Hagaman, *J. Am. Ceram Soc.* **74**, 1686 (1991).
11. P. Gozalez, R. Soto, E. G. Parada, X. Redondas, S. Chiussi, J. Serra, J. Pou, B. Leon, and M. Perz-Amor, *Appl. Surf. Sci.* **109**, 380 (1997).
12. H. Han and B. J. Feldman, *Solid State Commun.* **65**, 921 (1997).
13. B. Mitu, *Appl. Surf. Sci.* **184**, 96 (2001).
14. R. C. DeVries, *Mater. Res. Innov.* **1**, 161 (1997).
15. Y. A. Li, S. Su, H. S. Li, and W. Y. Luo, *J. Mater. Sci. Lett.* **17**, 31 (1998).
16. J. P. Riviere, D. Texier, J. Delafond, M. Jaonen, E. L. Mathe, and J. Chanmont, *Mater. Lett.* **22**, 115 (1995).
17. T. Sato, Furuno, S. Iguchi, and M. Hanabusa, *Appl. Phys. A* **45**, 355 (1988).
18. S. P. Lee, J. B. Kang, and S. Chowdhury, *J. Kor. Phys. Soc* **39**, S1 (2001).
19. M. Friedrich, T. Welzel, R. Rochotzki, H. Kupfer, and D. R. T. Zahn, *Diamond Relat. Mater.* **6**, 33 (1997).
20. S. E. Rodil, and A. C. Ferrari, J. Robertson and S. Muhl, *Thin Solid Films* **420-421**, 122 (2002).
21. S. P. Lee, and J. B. Kang, *Microchem. J.* **70**, 239 (2001).
22. C. Jama, V. Rousseau, O. Dessaux, and P. Goudmand, *Thin Solid Films* **302**, 58 (1997).
23. R. Alexandrescu, F. Huisken, A. Crunteanu, S. Petcu, S. Cojocaru, S. Cireasa, and I. Morjan, *Appl. Phys. A* **65**, 207 (1997).
24. M. Kohzaki, A. Matsumuro, T. Hayashi, M. Muramatsu, and K. Yamaguch, *Thin Solid Films* **308-309**, 239 (1997).
25. H. W. Song, F. Z. Cui, X. M. He, W. Z. Li, and H. D. Li, *J. Phys. Conden. Matt.* **6**, 6125 (1994).
26. S. Chowdhury, D. C. Carmeron, and M. S. J. Hashmi, *Surf. Coat. Tech.* **116-119**, 46 (1999).